Batteries & Supercaps

Research Article
doi.org/10.1002/batt.202300353

Chemistry Europe
European Chemical Societies Publishing

www.batteries-supercaps.org

Fluorinated Carbonate-aided Ionic-liquid Electrolyte Enables High-capacity Lithium-metal Batteries

Pengfei Liu,[a] Yuxin Rao,[a] Huasong Wang,[a] Xue Li,[a] Xiaomin Wang,[b] Miaomiao Yu,[a] Yong Li,[a] Zhihao Yue,[c] Fanglin Wu,*[d] and Shan Fang*[a]

Ionic liquids (ILs) are promising electrolyte candidates for high-safety and stability lithium metal batteries. However, their practical application is hindered by high viscosity resulting in a poor wettability of separator and sluggish Li^+ transport at room temperature. Herein, a weakly-solvating solvent of methyl (2,2,2-trifluoroethyl) carbonate (FEMC) is employed as a co-solvent in non-flammable ionic-liquid electrolyte (ILE) which composed with N-butyl-N-methylpyrrolidinium bis (fluorsulfonyl) imide ($Pyr_{14}FSI$) and bis (trifluoromethanesulfonyl) sulfonimide lithium salt (LiTFSI), effectively ameliorates the shortcomings of ILs mentioned above without sacrificing its safety character. Compared with pure ILE, the addition of FEMC can distinctly decrease the polarization voltage and electrode-electrolyte interface resistance. With the assistance of FEMC solvent, the discharge specific capacity of Li||$LiFePO_4$ (LFP) and Li||$LiNi_{0.6}Co_{0.2}Mn_{0.2}O_2$ (NCM622) cells are significantly improved. The origin of this great improvement is contributed to the exceptionally stable and LiF-rich cathode electrolyte interphase (CEI) layer formed in this electrolyte. Additionally, Li||$LiNi_{0.8}Co_{0.1}Mn_{0.1}O_2$ (NCM811) cells exhibit a remarkable rate capability (105 mAh g^{-1} at 2 C rate), achieve an initial specific capacity of 202.8 mAh g^{-1} and outstanding capacity retention of 88.2% over 100 cycles.

Introduction

In recent years, with the increasing popularity of electric vehicles (EVs), there is a pressing need to promote the development of energy storage systems (ESSs) and electrochemical energy systems (EESs).[1,2] Lithium metal batteries are the key to achieve the targets of carbon emission peak and neutrality owning to their substantial merits including high specific-capacity, long lifespan and environmental friendliness.[3] However, conventional carbonate-based electrolytes undergo inevitable side reaction with high-activity metallic lithium, resulting in the formation of an unstable solid electrolyte interphase (SEI).[4–10] The unstable SEI can hardly inhibit the chemical/electrochemical side reactions between lithium metal anode and electrolyte, which leads to the continuous consumption of electrolyte following by a growth of lithium dendrites, finally pierce the separator, causing the short circuit of cells. Additionally, the disconnected lithium dendrites generate "dead lithium", resulting in an irreversible capacity degradation of cells.[11–16]

Ionic liquids exhibit high thermal stability, nonvolatility and low-flammability at room temperature.[17–19] Bis (trifluoromethanesulfonyl) sulfonimide ($TFSI^-$) and bis (fluorosulfonyl) imide (FSI^-) are the common anions of ILs-based electrolytes for lithium metal batteries and were reported equipping with a synergistic effect, enabling a highly favorable interfacial passivation layers on the electrodes surface, and thereby dramatically improved electrochemical cycling stability.[20] With respect to the cations, pyrrolidinium-based cations are deemed to a promising choice that can afford sufficiently wide electrochemical window for high-voltage Li metal batteries,[21] such as 1-butyl-1methylpyrrolidinium (Pyr_{14}^+). However, its relatively high viscosity and low lithium-ion transference number limit the rate capability, and only allows the cell operating at a low mass loading or high operating temperature. A variety of strategies have been reported to resolve the issues, such as co-solvents,[22] electrolyte additives,[23] localized high concentration electrolytes (LHCEs),[24] The exploitation of non-solvating diluents is a remarkable strategy to address the above challenges, which can enhance the Li^+ transference number and contribute a more robust SEI layer on lithium metal anode.[25] Nevertheless, most diluents are belong to ethers group,[26] which behaves a poor high voltage resistance. In a comparison, fluorinated weakly-solvating co-solvent could be a more applicable solvent for IL considering it not only adjust the solvation behavior but also owns high voltage resistance. Among these, methyl (2,2,2-trifluoroethyl) carbonate (FEMC) as a weakly-solvating solvent

[a] P. Liu, Y. Rao, H. Wang, X. Li, M. Yu, Prof. Y. Li, Prof. S. Fang
School of Physics and Materials Science
Nanchang University
Nanchang 330031 (China)
E-mail: fangshan@ncu.edu.cn

[b] X. Wang
State Key Laboratory of Space Power Sources
Shanghai Institute of Space Power-Sources
Shanghai 200245 (China)

[c] Prof. Z. Yue
Institute of Photovoltaics
Nanchang University
Nanchang 330031 (China)

[d] Dr. F. Wu
State Key Laboratory of Advanced Technology for Materials Synthesis and Processing
Wuhan University of Technology
Wuhan 430070 (China)
E-mail: fanglin-wu@whut.edu.cn

Supporting information for this article is available on the WWW under https://doi.org/10.1002/batt.202300353

Research Article
doi.org/10.1002/batt.202300353
Chemistry Europe
European Chemical Societies Publishing

behaves an excellent chemical stability in high voltage battery system, has been widely joined the development of high voltage electrolyte.[27,28] FEMC is a fluorination of ethyl methyl carbonate (EMC) which demonstrates an excellent performance as co-solvent. The viscosity of FEMC is ~1.6 cP[29] much lower than the pure ILE (3LiTFSI-4Pyr$_{14}$FSI) of >300 cP.[30] Therefore, the introduction of FEMC as co-solvent in ILE will much reduce the viscosity of ILE. Based on the previous work, co-solvent could improve Li^+ transference number to some extent.[30] Additionally, its outstanding flame resistance guarantees no sacrifice to the thermal stability of ILs. Consequently, FEMC would be an ideal choice for the designing a more applicable ILE. In this work, the FEMC was selected as a co-solvent to assist LiTFSI-Pyr$_{14}$FSI electrolytes. A series of electrolytes are designed according to the different molar ratios of Li^+, Pyr_{14}^+ and FEMC, namely $[LiTFSI]_3[Pyr_{14}FSI]_4$ (ILE), $[LiTFSI]_3[Pyr_{14}FSI]_4[FEMC]_4$ (ILEF344) and $[LiTFSI]_3[Pyr_{14}FSI]_4[FEMC]_8$ (ILEF348), respectively. The optimized electrolyte, ILEF348, can effectively reduce the polarization voltage and the interface resistance between the electrolyte and lithium electrode, leading to the discharge specific capacity of Li||$LiFePO_4$ (LFP) cells was significantly improved from 50 mAh g^{-1} to 150 mAh g^{-1}. The similar results can be also obtained in Li||$LiNi_{0.6}Co_{0.2}Mn_{0.2}O_2$ (NCM622) and Li||$LiNi_{0.8}Co_{0.1}Mn_{0.1}O_2$ (NCM811) cells. Furthermore, the structural variation of cathode and cathode electrolyte interphase (CEI) were deeply investigated to elucidate the effect from weakly-solvating solvent.

Results and Discussion

Electrochemical performance of Li||Li symmetric cells

To evaluate the effect of FEMC as co-solvent on the interface between electrolyte and Li metal, Li||Li symmetrical cells were assembled to investigate the Li plating/stripping behavior upon cycling. As shown in Figure 1(a), the current density was set as 0.5 mA cm^{-2} and each plating or stripping process was confined to 1 hour. A much larger overpotential was observed for the ILE, followed by a gradual decrease accompanying with certain fluctuation, indicates the lithium dendrites were growing during the plating/stripping process. In a comparison, the ILEF344 and ILEF348 show a lower overpotential of ~100 mV following more stable cycling performance than ILE under long-term cycling. Then the current density was increased to 1 mA cm^{-2}, both ILEF344 and ILEF348 demonstrate steady cycling for 150 h, the overpotential is kept below 600 mV, and the value of ILEF348 is always lower than that of ILEF344 (Figure 1b). In contrast, the polarization voltage of the symmetric cells in ILE exhibits a sharp rise beyond 5 V during the first charging process (Figure S1), which could attribute to the high viscosity of pure ILE cannot adapt to high current density, result in slow ion transport dynamics and large polarization. In addition, the ILEF348 displays a significantly higher exchange current density (2.34 mA cm^{-2}) than the ILEF344 (0.58 mA cm^{-2}) and ILE (0.37 mA cm^{-2}) in Tafel plots (Figure 1c), indicating crucially fast charge exchange and rapidly electrochemical redox rection in

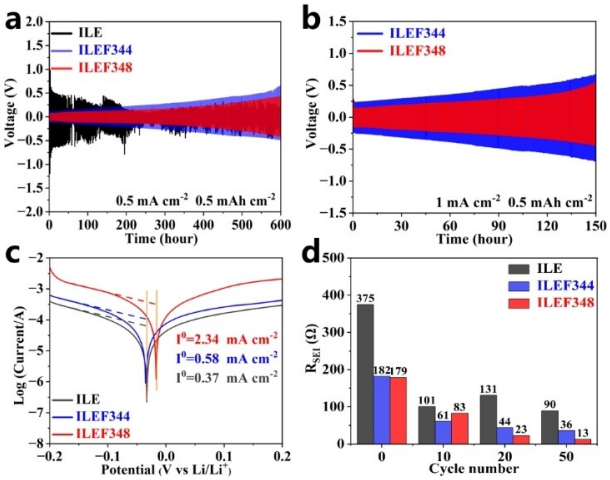

Figure 1. Electrochemical performances of Li||Li symmetric cells in various electrolytes. The long-term performances of Li||Li symmetric cells at different current densities of a) 0.5 mA cm^{-2}, b) 1 mA cm^{-2}. Capacity: 0.5 mAh cm^{-2}. c) Tafel plots of the three Li||Li symmetric cells before cycling. d) Comparison of R_{SEI} resistance values of various electrolytes at different cycles.

ILEF348. Electrochemical stability window was evaluated by linear sweep voltammetry (LSV) measurement with Swagelok cells (Figure S2). The cell using ILEF348 behaves a slightly higher voltage stability than ILEF344 (5.2 vs. 5.0 V), although difficult to compare with ILE which shows an excellent electrochemical stability up to 6.0 V. Besides, the results of the flammability test showed that the addition of FEMC did not make ILE lose its characteristics of non-flammability at room temperature. ILE continued to burn for a few seconds after the fire ignition lighter was removed. Although ILEF344 and ILEF348 were also flammable, they were both extinguished immediately after the fire ignition lighter was removed. (Figure S3). Electrochemical impedance spectroscopy (EIS) measurements were carried out to further study the influence of the FEMC on lithium-ion transport in Li||Li symmetrical cells (Figure S4). The ILEF348 exhibits the lowest bulk resistance (R_b) values among the three electrolytes (Figure S4), which may reflect a lower ionic conductivity of ILEF348. A continually decrease trend of SEI layer resistance (R_{SEI}) values with cycling was observed in all electrolytes (Figure 1d). Compared with ILE and ILEF344, a lowest R_{SEI} value shows in ILEF348. The lower R_{SEI} values of ILEF348 indicates FEMC solvent can facilitate Li^+ dissociation and transport at the electrode/electrolyte interface in the Li||Li symmetrical cells.

Cycling performance of Li||LFP and Li||NCM622 cells

The above results proved FEMC as a co-solvent are beneficial to improve the Li^+ transport in ILE. To evaluate the compatibility of ILE and FEMC-aided ILE in the full cells, LFP and NCM622 were selected as the cathodes, respectively. As shown in Figure 2, the Li||LFP cells assembled with high areal loading (~9.9 mg cm^{-2}) of the LFP and a Li foil (400 μm) as anode

Research Article
doi.org/10.1002/batt.202300353

Chemistry Europe
European Chemical Societies Publishing

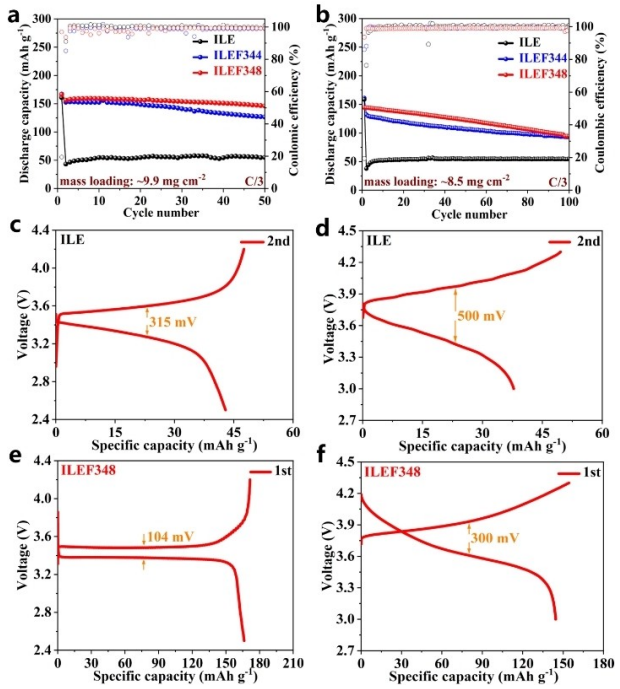

Figure 2. Electrochemical performance of Li||LFP and Li||NCM622 cells in different electrolytes. Cycling performance of a) Li||LFP and b) Li||NCM622 cells with the voltage range of 2.5–4.2 V and 3.0–4.3 V, respectively. Selected charge/discharge curve of Li||LFP cells in c) ILE and e) ILEF348. Selected charge/discharge voltage curve of the Li||NCM622 cells in ILE (d) and ILEF348 (f). All cells are charged to cutoff voltage with initial cycle at 0.1 C, and then at a current density of 1/3 C.

electrode with the voltage range of 2.5–4.2 V. The cells with ILE endure an overcharge state with much higher capacity during the first charge process (Figure S5a), which indicates the ILE is unstable at the high voltage plateau in the high mass loading electrode, resulting in a continual side reaction at the electrode/electrolyte interface. When the charge current was increased to 1/3 C in the subsequent cycles, the discharge capacity decreases to only about 50 mAh g^{-1} after 50 cycles. This is due to the slow Li^+ diffusion kinetics and transport at the interface resulting in a large cell polarization, thereby reducing the cell's discharge capacity. In a comparison, the FEMC-aided ILEs deliver a dramatically higher capacity above 150 mAh g^{-1} at 1/3 C, which almost triple than the value of ILE. The electrochemical results confirm the FEMC co-solvent could obviously enhance Li^+ diffusion kinetics and reduce the cell polarization. The voltage curves well demonstrate much larger polarization voltage in ILE than ILEF348 (315 mV vs. 104 mV in Li||LFP cells, Figure 2c, e), a relatively low value is also presented in ILE344 (Figure S6). The cells cycled in ILEF348 delivers a desirable capacity retention of 93.0% and discharge capacity of 146 mAh g^{-1} after 50 cycles, which are higher than these cells cycled in ILEF344 (87.0%, 134 mAh g^{-1}). The EIS results showed that the R_b and R_{SEI} of two FEMC-assisted electrolytes are significantly lower than ILE, indicating a greatly improvement on the Li^+ transport kinetics in these electrolytes (Figure S7a–c). A similar experimental result is displayed in Li|| NCM622 cells using ILE. The first activation process still displays an overcharge behavior (Figure S5b), then the discharge curve of the cells linearly drops to around 50 mAh g^{-1}. In contrast, the first activation cycle of using the ILEF344 and ILEF348 cells achieves discharge capacity of 161 mAh g^{-1} and 144 mAh g^{-1}, respectively (Figure 2b). Both of their average CE exceed 99.0% after 100 cycles. The above experimental results demonstrate that the introduction of FEMC can not only reduce the R_b and R_{SEI}, but also help to form a stable CEI layer to prevent continual side reactions, achieve a higher CE and enhanced cycling reversibility of cells.

Electrochemical behaviour of Li||NCM811 cells

As shown in Figure 3(a), the cells with ILE experience a clear decay during 100 cycles, retaining only 65.0% of the initial capacity with an average CE of 88.7%. Simultaneously, the polarization of cells is significantly increased after first cycling (Figure S8), this indicates the formation of an unstable CEI layer on the surface of electrode, leading to the poor compatibility between NCM811 and ILE. After using ILEF344 and ILEF348, the average CE of cells are improved to 99.0% and 98.0%, respectively. The cell polarization is greatly reduced as well (Figure 3b). Figure 3(c) displays the rate performances with a succession of current rate of 0.1 C, 0.2 C, 0.5 C, 1 C, 2 C, and 0.1 C at 4.3 V. Obviously, the advantages of ILEF348 are brought into fully play at different rates, especially at high rates, achieving the superior discharge capacities of 174, 144, and 105 mAh g^{-1} at 0.5 C, 1 C and 2 C, respectively, as compared to the values of 160, 130 and 95 mAh/g of ILEF344, and 177, 85 and 43 mAh g^{-1} of ILE, respectively. In Figure 3(d), the superiority of ILEF348 on the interfacial characteristics of Li||NCM811 cells are evaluated by EIS. Before cycling, the Nyquist curves of ILEF348-based cells exhibit lower interface resistances of R_b and

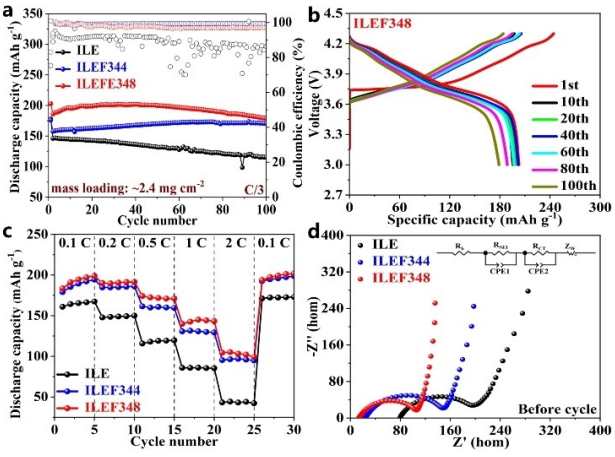

Figure 3. Electrochemical performance of Li||NCM811 cells in various electrolytes. a) Cycling comparison of Li||NCM811 cells between 3.0–4.3 V in the three electrolytes. b) Electrochemical charge/discharge curves of the Li||NCM811 cells between 3.0–4.3 V in ILEF348. c) Rate capability of the Li||NCM811 cells between 3.0–4.3 V at different rates. d) Nyquist plots of the Li||NCM811 cells in various electrolytes before cycle. All cells are charged to cutoff voltage with initial cycle at 0.1 C, followed by 1/3 C cycling.

Research Article
doi.org/10.1002/batt.202300353
Chemistry Europe
European Chemical Societies Publishing

R_{SEI} than ILE and ILEF344. After 100 cycles at 1/3 C, the impedance (R_b and R_{SEI}) of the cells cycled in ILEF344 are lower than those of the cells cycled in ILE and ILEF348 (Figure S9), confirming the formation of the high-conductivity SEI layer of the cells cycled in the ILEF344.

Morphology analysis of the cycled electrodes

To determine the effect from the electrolytes to different performance of LFP, NCM622 and NCM811 electrodes cycled in the three electrolytes (ILE, ILEF344 and ILEF348), the morphology of LFP, NCM622 and NCM811 electrodes before and after cycling were investigated (Figure 4). Due to the low ionic conductivity of the ILE, achieves an efficient Li^+ plating/stripping becomes challenging. The plating/stripping process of Li^+ induces volume expansion/contraction in the secondary particles. If the secondary particles cannot effectively accommodate these volume changes, stress concentration may lead to crack formation after cycling. The experimental results indicate that ILE cannot form a robust solid electrolyte interphase on the cathode surface, resulting in particle fracture (Figure 4d–f). Figure 4(h) exhibits that ILEF344 is hard to effectively avoid this disadvantage, and cracks still exist at the edge of the particles. In contrast, this phenomenon is not observed for the particles of the electrodes cycled in ILEF348 (Figure 4j–l), which essentially appear as the fresh electrodes (Figure 4a–c). The surface of electrodes which cycled in ILEF348 appear smooth and can be well protected, indicating that a more stable and robust CEI layer on the surface.

In order to evaluate the effect for the inner structure of particles occurring upon cycling in the three electrolytes, the inner secondary particle morphology was investigated by acquiring SEM cross-sectional images after focused ion-beam (FIB) cutting and polishing. The fresh particles exhibit a well-structured shape without any microcrack visible (Figure 5a). However, some cracks are clearly seen in the partial particles cycled in ILE (Figure 5b), penetrating from the surface into the core along the grain boundaries of the primary particles. There are a small number of cracks in the NCM622 particles after 100 cycles in ILEF344 and ILEF348 electrolytes, but the number of cracks and the degree of particle cracking are smaller than those of ILE (Figure 5c, d), indicating that the addition of FEMC can form a CEI layer with certain protection ability. To further prove the stability of the ILEF348-derived CEI layer, the self-discharge test is shown in Figure S10. The NCM622 electrode with ILEF348 could maintain around 3.5 V after storing for 24 hours without serious voltage degradation, indicating a relatively stable CEI layer on the NCM622 surface.[31]

The surface chemistry of cycled cathodes

To investigate the role of the FEMC co-solvent on the compositional variation of CEI layer on the LFP electrode, X-ray photoelectron spectroscopy (XPS) analysis was performed after 150 cycles (Figure 6). In the C 1s spectrum for the three electrolytes, the major peak at 284.8 eV is attributed to C–C/C–H species of carbon black and PVDF. The peak located at around 286.4 eV, assigned to C–N/C–O–C, originates from the decomposition of Pyr_{14}^+. Since none of the three ions (Pyr_{14}^+, FSI^- and $TFSI^-$) contains O–C=O/C=O, its presence indicates the occurrence of FEMC decomposition during the CEI formation on cathodes. Furthermore, an appearance of a new peak at 293.0 eV (Figure 6d and g), attributed to -CF_3 containing functionalities, certifies the FEMC decomposition as well. The tiny peak at 291.0 eV in Figure 6(a) originates from $TFSI^-$. In the N 1s spectra, the peaks at 400.3 eV and 402.7 eV correspond to FSI^-/$TFSI^-$ and Pyr_{14}^+, respectively. In the F 1s spectra, a small peak at 685.0 eV is LiF in Figure 6(c),[32] which is generated due

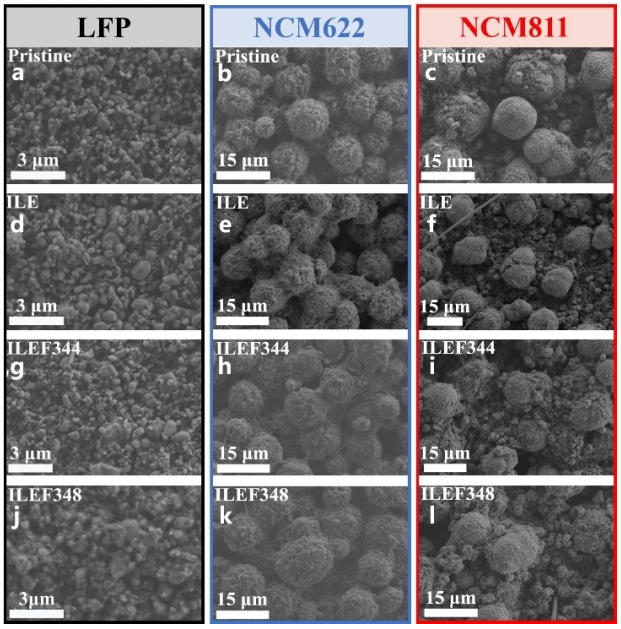

Figure 4. Morphological analysis of cycled LFP, NCM622 and NCM811 electrodes. a-c) Top-view SEM micrographs of pristine (fresh) electrodes, as well as electrodes, after 100 cycles of NCM622 and NCM811, 150 cycles of LFP (at 1/3 C) in d-f) ILE, g–i) ILEF344 and j-l) ILEF348.

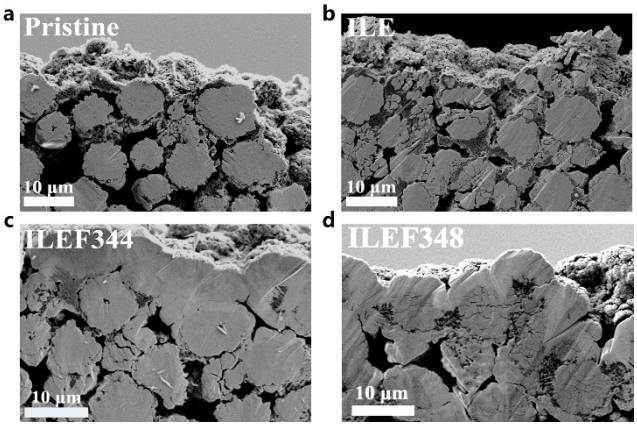

Figure 5. The cross-sectional of morphological analysis of cycled NCM622 electrodes. Cross-sectional SEM micrographs of a) pristine (fresh) NCM622 electrode, as well as NCM622 electrodes, after 100 cycles (at 1/3 C) in b) ILE, c) ILEF344 and d) ILEF348.

Research Article
doi.org/10.1002/batt.202300353
Chemistry Europe
European Chemical Societies Publishing

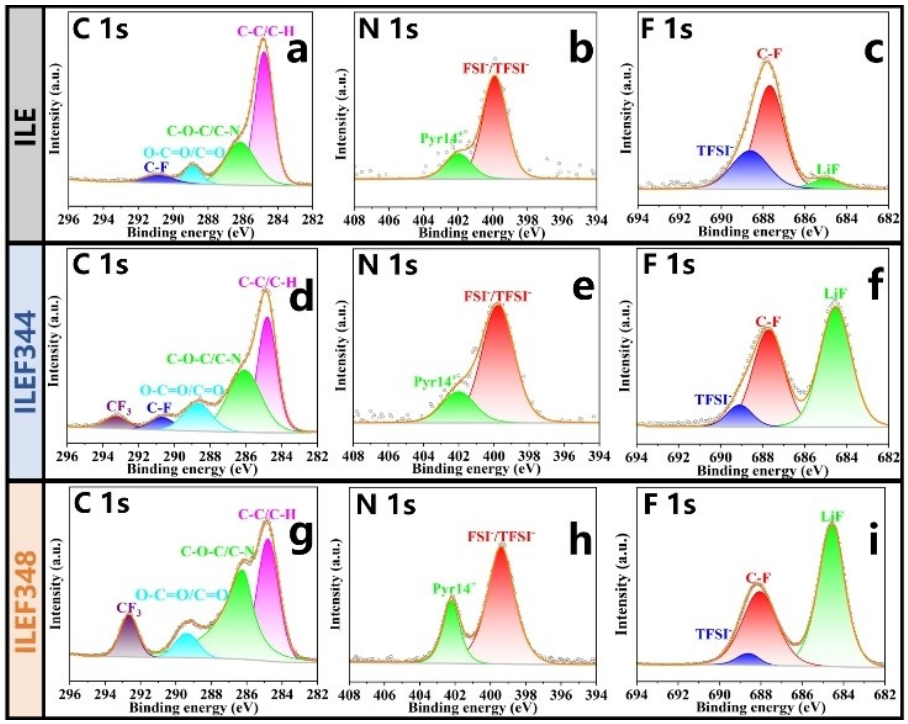

Figure 6. Characterization of the CEI layer on LFP after cycling. XPS analysis of LFP electrodes after 150 cycles in a–c) ILE, d–f) ILEF344 and g–i) ILEF348.

to the decomposition of FSI^-/$TFSI^-$. In contrast, the LiF content in ILEF344 and ILEF348 (Figure 6f and i) is significantly higher than ILE, indicating that FEMC contributes to the generation of LiF in the CEI layer. Although LiF can effectively suppress the anode interface reactions and provide a stable protective layer in batteries.[35] However, due to LiF is an electric insulator, excessive LiF content may lead to decreased ion conductivity and increased internal impedance of the battery. The main feature appears in the O 1s region (peak at 532.4 eV due to the O=S=O group), which is clearly associated to the presence of LiTFSI and its decomposition products in the CEI (Figure S11a). In the S 2p spectra, NSO_2 and $FNSO_2$ peaks at 168.3 eV and 171.3 eV are also observed respectively (Figure S11b), which come from the decomposition of FSI^-/$TFSI^-$. Additionally, the CEI layer formed in ILEF344 and ILEF348 contains LiNSO (163.8 eV) and Li_xSO_y (166.6 eV) are identified which have a beneficial influence on its stability because of their electronically insulating and ion conducting properties.

Conclusions

In this work, FEMC is employed as a co-solvent for the ILE to enhance the cycling stability as well as structural stability of cathode materials, such as LFP, NCM622 and NCM811. Morphological and chemical analysis indicate that the introduction of FEMC can effectively form a LiF-rich layer, which effectively suppress the cracking of secondary particles and contribute to enhanced battery performances compared to ILE. The use of ILEF348 in Li||NCM811 cells exhibit excellent average CE above 99.0%, satisfied rate capability (102 mAh g^{-1} at 2 C rate) and outstanding capacity retention of 88.2% over 100 cycles. The discovery of FEMC as a co-solvent will give insights into the further developing IL-based electrolytes for high safety and more practical LMBs.

Experimental Section

Preparation of the electrolytes and electrode materials

The 1-butyl-1-methylpyrrolidinium bis (fluorosulfonyl) imide ($Pyr_{14}FSI$, ≥98.0%), Bis (trifluoromethanesulfonyl) sulfonimide lithium salt (LiTFSI, ≥99.9%), and methyl (2,2,2-trifluoroethyl) carbonate (FEMC, ≥98.0%) were obtained from Aladdin without further purification before using. LiTFSI salt was dried at 120 °C for 24 h under vacuum and the electrolytes were formulated in an Ar-filled glove box with both oxygen and water below 0.1 ppm. The ILE was prepared by mixing LiTFSI and $Pyr_{14}FSI$ in a molar ratio of 3:4. FEMC-aided electrolytes were made by mixing LiTFSI, $Pyr_{14}FSI$ and FEMC in 3:4:4 and 3:4:8 molar ratio, hereinafter denoted as "ILEF344" and "ILEF348". Li metal disks were provided by China Energy Lithium Co. Ltd (thickness: 400 μm, diameter: 12 mm or 16 mm) that stored in an Ar-filled glove box. The Whatman GF/D separator was bought from Cytiva.

The $LiFePO_4$ (LFP) and $LiNi_{0.6}Co_{0.2}Mn_{0.2}O_2$ (NCM622) cathodes were purchased from Guangdong Canrd New Energy Technology Co. Ltd. The average mass loading of the LFP and NCM622 cathodes were calculated as about 8.5–10.0 mg cm^{-2}. The preparation of the $LiNi_{0.8}Co_{0.1}Mn_{0.1}O_2$ (NCM811) electrode involves mixing NCM811 powder, conductive carbon black, Poly (vinylidene fluoride) (PVDF) with a weight ratio of 92:4:4, 1-methyl-2-pyrrolidinone (NMP) was used as solvent to form a slurry, then coated onto an Al foil. Vacuum drying at 120 °C for 12 hours. To punched into a diameter of 12 mm disc as positive electrode. The average mass loading of

active material in the NCM811 positive electrode is around 2.4 mg cm^{-2}.

Electrochemical measurements

The electrochemical performances were tested in the CR2025 coin-type Li||Li symmetrical cells, Li||LFP, Li||NCM622 and Li||NCM811 cells. The battery assembly was performed in an Ar-filled glove box with both oxygen and water below 0.1 ppm. The cathodes and anodes were separated by a Whatman DF/D membrane soaked with 120 μL electrolyte. The Li||Li symmetrical cells were cycled at 0.5 mA cm^{-2} and 1 mA cm^{-2} with a deposition capacity of 0.5 mAh cm^{-2}. The cells were run at a low current of 0.1 C for the initial activation to form a stable interphase on Li||LFP, Li||NCM622 and Li||NCM811 cells, following a cycling test at 1/3 C (1 C = 150, 178 and 200 mA g^{-1}, respectively), the voltage windows of the Li||LFP cell was 2.5–4.2 V, the Li||NCM622 and Li||NCM811 cells was 3.0–4.3 V. All the cells were tested using Land battery test system (CT3002 A, Wuhan, China) at 25 °C. The LSV and EIS (5 mV, 10^5–10^{-2} Hz) measurements were carried out using electrochemical work station (CHI660E, Shanghai, China).

Materials characterization

All characterized electrodes were obtained by disassembling the cycled cells, the electrode samples were rinsed three times with dimethyl carbonate (DMC) and then thoroughly dried under vacuum. The fielded emission scanning electron microscope (FESEM, Sigma 300VP) was applied to observe the morphology of cycled electrodes. XPS with Al K_α X-ray radiation (ESCALAB 250Xi, ThermoFischer, America) was employed to investigate the detailed information on chemical compositions.

Acknowledgements

Project funded by the National Natural Science Foundation of China (52002176, 52161039), Jiangxi Provincial Natural Science Foundation (20212BAB214054, 20224BAB204011, 20212BAB214053, 20223BBE51028, 20223BBE51022). Project of academic and technical leaders of main disciplines in Jiangxi Province (20212BCJ23041), Talent Project of Double Thousands Plan in Jiangxi Province (jxsq2023201093), Talent project of double hundred and double thousand plan in Jiujiang City (jjsbsq20210004).

Conflict of Interests

The authors declare no conflict of interest.

Data Availability Statement

The data that support the findings of this study are available from the corresponding author upon reasonable request.

Keywords: FEMC · weakly-solvating solvent · ionic liquid electrolytes · cathode electrolyte interphase · lithium metal batteries

[1] L. R. Hou, R. Q. Bao, Y. R. Zhang, X. Sun, J. Y. Zhang, H. Dou, X. G. Zhang, C. Z. Yuan, *J. Mater. Chem. A* **2018**, *6*, 17947.
[2] Z. L. Wang, D. K. Denis, Z. W. Zhao, X. Sun, J. Y. Zhang, L. R. Hou, C. Z. Yuan, *J. Mater. Chem. A* **2019**, *7*,18109.
[3] J. Lin, X. D. Zhang, E. S. Fan, R. J. Chen, F. Wu, L. Li, *Energy Environ. Sci.* **2023**, *16*, 745.
[4] S. H. Jiao, X. D. Ren, R. G. Cao, M. H. Engelhard, Y. Z. Liu, D. H. Hu, D. H. Mei, J. M. Zheng, W. G. Zhao, Q. Y. Li, N. Liu, B. D. Adams, C. Ma, J. Liu, J. G. Zhang, W Xu, *Nat. Energy* **2018**, *3*, 739–746.
[5] S. M. Chen, K. H. Wen, J. T. Fan, Y. Bando, D. Golberg, *J. Mater. Chem. A* **2018**, *6*, 11631.
[6] D. J. Yoo, S. Y. Yang, K. J. Kim, J. W. Choi, *Angew. Chem. Int. Ed.* **2020**, *59*, 14869–14876.
[7] W. N. Zhang, T. Yang, X. B. Liao, Y. Song, Y. Zhao, *Energy Storage Mater.* **2023**, *57*, 249–259.
[8] S. Fang, F. L. Wu, S. Q. Zhao, M. Zarrabeitia, G. T. Kim, J. K. Kim, N. G. Zhou, S. Passerini, *Adv. Energy Mater.* **2023**, 2302577, https://doi.org/10.1002/aenm.202302577.
[9] D. Jin, C. Park, J. Han, C. B. Dzakpasu, E. Kim, J. Oh, K. M. Kim, S. Lee, Y. M. Lee, *Bat. Energy* **2023**, *2*, 20220034.
[10] Y. G. Zou, G. Liu, Y. Q. Wang, Q. Li, Z. Ma, D. M. Yin, Y. Liang, Z. Cao, L. Cavallo, H. Kim, L. M. Wang, H. N. Alshareef, Y. K. Sun, J. Ming, *Adv. Energy Mater.* **2023**, *13*, 2300443.
[11] Y. Y. Lu, K. Korf, Y. Kambe, Z. Y. Tu, L. A. Archer, *Angew. Chem. Int. Ed.* **2014**, *53*, 488–492.
[12] W. B. Wu, Y. Y. Bo, D. P. Li, Y. H. Liang, J. H. Zhang, M. M. Cao, R. T. Guo, Z. Y. Zhu, L. J. Ci, M. Y. Li, J. H. Zhang, *Nano-Micro Lett.* **2022**, *14*, 44.
[13] K. Yue, C. X. Zhai, S. N. Gu, J. J. Yeo, G. W. Zhou, *Electrochim. Acta.* **2022**, *401*, 139527.
[14] Z. A. Yu, H. S. Wang, X. Kong, W. Huang, Y. Tsao, D. G. Mackanic, K. C. Wang, X. C. Wang, W. X. Huang, S. Choudhury, Y. Zheng, C. V. Amanchukwu, S. T. Hung, Y. T. Ma, E. G. Lomeli, J. Qin, Y. Cui, Z. N. Bao, *Nat. Energy* **2020**, *5*, 526–533.
[15] Z. A. Yu, P. E. Rudnicki, Z. W. Zhang, Z. J. Huang, H. Celik, S. T. Oyakhire, Y. L. Chen, X. Kong, S. C. Kim, X. Xiao, H. S. Wang, Y. Zheng, G. A. Kamat, M. S. Kim, S. F. Bent, J. Qin, Y. Cui, Z. N. Bao, *Nat. Energy* **2022**, *7*, 94–106.
[16] M. Wu, Z. Y. Wang, W. R. Zhang, C. Jayawardana, Y. Li, F. Chen, B. Nan, B. L. Lucht, C. S. Wang, *Angew. Chem. Int. Ed.* **2023**, *62*, e202216169.
[17] F. L. Wu, M. Kuenzel, T. Diemant, A. Mullaliu, S. Fang, J. K. Kim, G. T. Kim, S. Passerini, *Small* **2022**, *18*, 2203874.
[18] F. L. Wu, A. R. Schür, G. T. Kim, X. Dong, M. Kuenzel, T. Diemant, G. D'Orsi, E. Simonetti, M. D. Francesco, M. Bellusci, G. B. Appetecchi, S. Passerini, *Energy Storage Mater.* **2021**, *42*, 826–835.
[19] F. L. Wu, G. T. Kim, T. Diemant, M. Kuenzel, A. R. Schür, X. P. Gao, B. S. Qin, D. Alwast, Z. Jusys, R. J. Behm, D. Geiger, U. Kaiser, S. Passerini, *Adv. Energy Mater.* **2020**, *10*, 2001830.
[20] F. L. Wu, S. Fang, M. Kuenzel, A. Mullaliu, J. K. Kim, X. P. Gao, T. Diemant, G. T. Kim, S. Passerini, *Joule* **2021**, *5*, 1–18.
[21] H. Sun, G. Z. Zhu, Y. M. Zhu, M. C. Lin, H. Chen, Y. Y. Li, W. H. Hung, B. Zhou, X. Wang, Y. X. Bai, M. Gu, C. L. Huang, H. C. Tai, X. T. Xu, M. Angell, J. J. Shyue, H. J. Dai, *Adv. Mater.* **2020**, *32*, 2001741.
[22] U. Pal, D. Rakov, B. Y. Lu, B. Sayahpour, F. F. Chen, B. Roy, D. R. MacFarlane, M. Armand, P. C. Howlett, Y. S. Meng, M. Forsyth, *Energy Environ. Sci.* **2022**,*15*,1907–1919.
[23] J. R. Nair, F. Colò, A. Kazzazi, M. Moreno, D. Bresser, R. Y. Lin, F. Bella, G. Meligrana, S. Fantini, E. Simonetti, G. B. Appetecchi, S. Passerini, C. Gerbaldi, *J. Power Sources* **2019**, *412*, 398–407.
[24] X. Liu, T. Diemant, A. Mariani, X. Dong, M. E. D. Pietro, A. Mele, S. Passerini, *Adv. Mater.* **2022**, *34*, 2207155.
[25] X. Liu, A. Mariani, H. Adenusi, S. Passerini, *Angew. Chem. Int. Ed.* **2023**, *62*, e202219318.
[26] S. Lee, K. Park, B. Koo, C. Park, M. Jang, H. Lee, H. Lee, *Adv. Funct. Mater.* **2020**, *30*, 2003132.
[27] Q. F. Zheng, Y. Yamada, R. Shang, S. Ko, Y. Y. Lee, K. Kim, E. Nakamura, A. Yamada, *Nat. Energy* **2020**, *5*, 291–298.
[28] X. L. Fan, L. Chen, O. Borodin, X. Ji, J. Chen, S. Hou, T. Deng, J. Zheng, C. Y. Yang, S. L, K. Amine, K. Xu, C. S. Wang, *Nat. Nanotechnol.* **2018**, *13*, 1191.

[29] M. Takehara, N. Tsukimori, N. Nanbu, M. Ue, Y. Sasaki, *Electrochemistry* **2003**, *71*,1201–1204.
[30] X. Liu, M. Zarrabeitia, A. Mariani, X. P. Gao, H. M. Schütz, S. Fang, T. Bizien, G. A. Elia, S. Passerini, *Small Methods* **2021**, *5*, 2100168.
[31] Z. Xie, J. He, Z. Y. Xia, Q. Q. Cai, Z. Y. Tang, J. Cai, Y. L. Chen, X. Q. Li, Y. Z. Fan, L. D. Xing, Y. B. Shen, W. S. Li, *J. Energy Chem.* **2023**, *86*, 197–207.
[32] X. F. He, X. Liu, Q. Han, P. Zhang, X. S. Song, Y. Zhao, *Angew. Chem. Int. Ed.* **2020**, *59*, 6397–6405.
[33] R. May, J. C. Hestenes, N. A. Munich, L. E. Marbella, *J. Power Sources* **2023**, *553*, 232299.
[34] D. Zhang, D. W. Zhu, W. Y. Guo, C. W. Deng, Q. J. Xu, H. X. Li, Y. L. Min, *Adv. Funct. Mater.* **2022**, *32*, 2112764.
[35] X. Liu, M. Zarrabeitia, A. Mariani, X. P. Gao, H. M. Schütz, S. Fang, T. Bizien, G. A. Elia, S. Passerini, *Small Methods* **2021**, *5*, 2100168.

Manuscript received: August 10, 2023
Revised manuscript received: September 27, 2023
Accepted manuscript online: October 23, 2023
Version of record online: November 13, 2023